ChemPubSoc Europe

DOI: 10.1002/cssc.201600117

CHEMSUSCHEM Communications

# Disordered 3D Multi-layer Graphene Anode Material from $CO_2$ for Sodium-Ion Batteries

Kassiopeia Smith,[a] Riley Parrish,[a] Wei Wei,[b] Yuzi Liu,[c] Tao Li,[d] Yun Hang Hu,[b] and Hui Xiong*[a]

We report the application of disordered 3D multi-layer graphene, synthesized directly from $CO_2$ gas through a reaction with Li at 550 °C, as an anode for Na-ion batteries (SIBs) toward a sustainable and greener future. The material exhibited a reversible capacity of ~190 mA h g$^{-1}$ with a Coulombic efficiency of 98.5% at a current density of 15 mA g$^{-1}$. The discharge capacity at higher potentials (>0.2 V vs. Na/Na$^+$) is ascribed to Na-ion adsorption at defect sites, whereas the capacity at low potentials (<0.2 V) is ascribed to intercalation between graphene sheets through electrochemical characterization, Raman spectroscopy, and small-angle X-ray scattering experiments. The disordered multi-layer graphene electrode demonstrated a great rate capability and cyclability. This novel approach to synthesize disordered 3D multi-layer graphene from $CO_2$ gas makes it attractive not only as an anode material for SIBs but also to mitigate $CO_2$ emission.

Over the last few decades, Li-ion battery (LIB) technology has dominated the portable electronics market and is considered the most promising energy storage system for use in electric vehicles and renewable energy storage. On the other hand, limited Li sources and growing cost[1–3] presents hindrance for LIBs in applications for power grid and large scale energy storage for intermittent renewable energy. As a result, alternative energy systems, such as Na-ion batteries (SIBs), have regained interest in recent years.[1,2,4–8]

Na has the advantage of low cost, owing to its global abundance and variety of source materials.[1–4,6,7] While Li and Na systems have many common attributes, key differences, including the ionic radius of Na (~1.02 Å) that is almost twice that of Li (~0.76 Å), present difficult challenges when trying to transition chemistries used for Li to applications with Na.[2,4–7,9–11] Suitable host materials need to be identified to accommodate Na ions and allow reversible Na-ion insertion and extraction.

Whereas substantial efforts have been made to identify suitable cathodes for SIBs with reversible capacities ranging from 50 to 200 mA h g$^{-1}$, there are limited choices for the anode.[2,4,8,12–14] Graphite, the most successfully used commercial anode material in LIBs, shows little to no capacity in SIBs, owing largely to the insufficient spacing (3.35 Å) between graphitic layers to form a stage-I intercalation compound ($LiC_6$).[15–17] A recent density functional theory (DFT) study showed that the stage-I binary graphite intercalation compound (GIC) structures, such as $NaC_6$ and $NaC_8$, an analogue to $LiC_6$, cannot be formed even through a vapor-phase intercalation reaction.[18] On the other hand, a recent work by Kang et al. showed that formation of ternary Na-intercalated GICs is possible by tailoring the length of the solvent species for co-intercalation.[19] Nevertheless, it is believed that large interlayer distance between the graphene sheets in carbonaceous materials is more energetically favorable to accommodate the insertion of Na$^+$ ions.[16,17,20] Hence, most studies of carbonaceous anode materials focused on disordered carbon, such as hard carbon materials, owing to their large interlayer distance and disordered structure, which facilitate Na-ion insertion/extraction.[21–23] Hard carbon materials display considerable capacities (150–300 mA h g$^{-1}$), but have unsatisfying cyclability and rate performance.[21–23] Nanostructured carbon, such as hollow carbon nanowire,[16] carbon nanosheet framework,[24] N-doped carbon nanofibers,[25] and N-doped graphene foams,[26] demonstrate improved rate performance owing to their short diffusion distance.

Herein, we report a disordered 3D multi-layer graphene (dMLG) material from $CO_2$ as a promising anode for SIBs. Recently, we developed a novel approach to create a unique type of dMLG directly from $CO_2$ through a simple reaction between Li liquid and $CO_2$ gas, which results in a cauliflower-fungus-like network of multi-layer graphene buckled on itself to create a 3D structure.[27] This approach not only enables the synthesis of dMLG, but can also mitigate $CO_2$ emission. Previous works show that these cauliflower-fungus-like dMLGs exhibit excellent electrocatalytic properties as a counter electrode for dye-sensitized solar cells.[27] In this work, dMLG anode synthesized from $CO_2$ gas exhibits a reversible capacity approximately 190 mA h g$^{-1}$ at a current density of 15 mA g$^{-1}$, retain-

[a] K. Smith, R. Parrish, Prof. H. Xiong
Micron School of Materials
Boise State University
1910 University Dr, Boise, ID, 83725 (USA)
E-mail: clairexiong@boisestate.edu

[b] W. Wei, Prof. Y. H. Hu
Department of Materials Science and Engineering
Michigan Technological University
1400 Townsend Drive, Houghton, MI, 49931-1295 (USA)

[c] Dr. Y. Liu
Center for Nanoscale Materials
Argonne National Laboratory
9700 S. Cass Avenue, Lemont, IL, 60439 (USA)

[d] Dr. T. Li
Advanced Photon Source
Argonne National Laboratory
9700 S. Cass Avenue, Lemont, IL, 60439 (USA)

Supporting Information and the ORCID identification number(s) for the author(s) of this article can be found under http://dx.doi.org/10.1002/cssc.201600117.

ing 98.4% of the initial capacity at a current rate of 750 mA $g^{-1}$ for 100 cycles and 81% at 500 cycles, and good rate capability. The novel approach to synthesize dMLG from $CO_2$ gas makes it attractive not only as an anode material for SIBs but also to control $CO_2$ emission.

The reaction of the Li liquid with $CO_2$ gas to form graphene-structured carbon is thermodynamically feasible based on the results from our previous work.[27] Graphite formation is prevented by simultaneous generation of $Li_2CO_3$ with graphene to isolate graphene sheets from each other during the synthesis. The as-prepared carbon sample exhibits a 3D cauliflower-fungus-like morphology with a sheet thickness of ~2 nm by scanning electron microscopy (SEM, Figure 1A). The laminated electrode mixed with carboxymethyl cellulose binder is shown in Figure 1B for comparison. It is clear that the 3D feature of graphene sheets is maintained in the laminated electrode. The layer structure of the as-prepared carbon was further confirmed by XRD (Figure 2A), which shows two broad peaks centered around $2\theta = 26^\circ$ and 45°, corresponding to the (002) and (100) planes, respectively. The average graphene interlayer spacing (3.51 Å) was calculated from the peak centers and is larger than the interlayer spacing of graphite (3.35 Å). The thickness ($L_c$) of the graphene layers (1.65 nm) was calculated based on Scherrer equation, using the full width at half-maximum (fwhm) value of the (002) plane. It is indicated that the graphene domains are composed of 4–5 stacked graphene layers (i.e., 1.65 nm/0.351 nm = 4.7), which is confirmed by high-resolution transmission electron microscopy (HRTEM, Figure 1D) as well. The HRTEM image also reveals that the sample is composed of disordered graphitic domains with a few-layer stacked-graphene sheets (Figure 1D and E). Furthermore, our previous X-ray photoelectron spectroscopy (XPS) measurement showed that the carbon sample consisted of 84% $sp^2$ carbon and 16% $sp^3$ carbon,[27] which further supports its graphene structure. However, the graphene material did not exhibit an electron diffraction pattern, revealing its highly disordered structure. Therefore, the graphene material is defined as dMLG. The material has a surface area of ~462 $m^2 g^{-1}$ from Brunauer–Emmett–Teller (BET) measurements and a pore size distribution ranging from 2 to 70 nm based on Barret–Joyner–Halenda (BJH) calculation (see the Supporting Information for details).

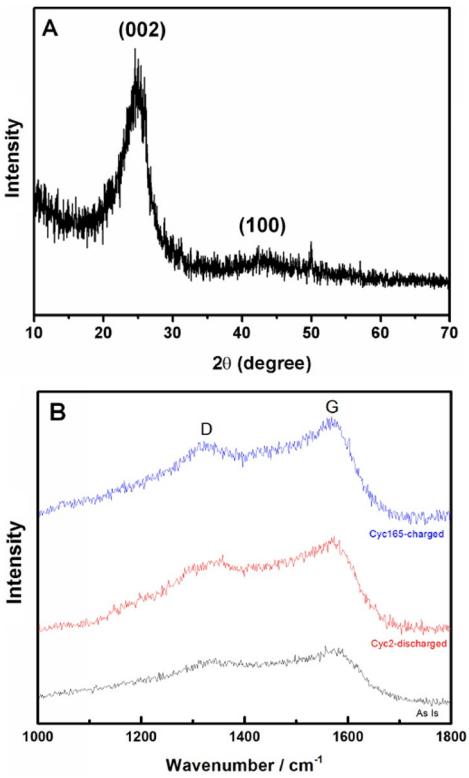


**Figure 2.** (A) XRD pattern of the as-prepared dMLG and (B) Raman spectra of the dMLG electrodes at different states of charge.

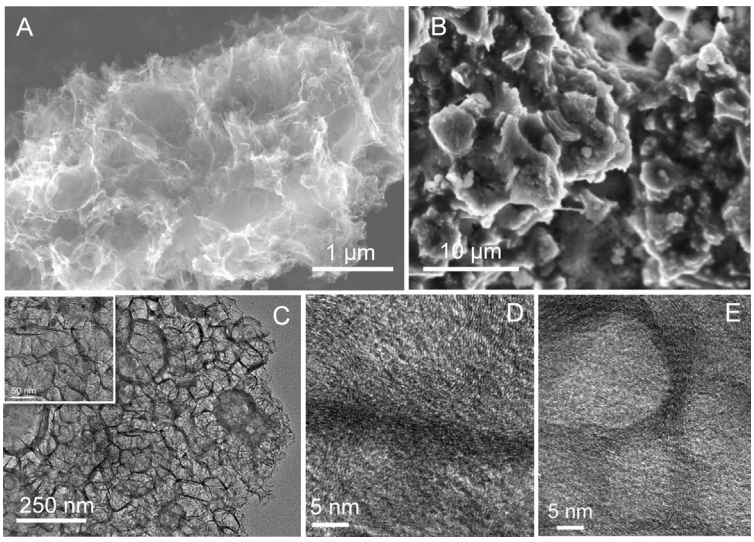


**Figure 1.** (A) SEM images of as-prepared 3D cauliflower-fungus-like dMLG and (B) laminated electrode. (C) TEM image of a discharged dMLG electrode (inset: a zoomed-in view. (D) HRTEM images of as-prepared disordered multi-layer graphene and (E) electrode cycled and stopped at the discharged (sodiated) state.

Raman spectroscopy was employed to investigate the disordered structure of the dMLG. Samples at different states of charge (i.e., as-prepared, 2nd discharge, and 165th charge) were evaluated. All samples exhibit a D band at 1350 $cm^{-1}$ (ascribed to disordered $sp^2$ carbon induced by the linking with $sp^3$ carbon atoms), and a G band at 1580 $cm^{-1}$ owing to in-plane vibrations of graphitic $sp^2$ carbons. The integrated intensity ratio ($I_D/I_G$) is used to estimate the degree of disorder in the carbons.[24,28] At discharged state, the electrode became more disordered upon Na-ion insertion indicated by the increased $I_D/I_G$ ratio ($I_D/I_G = 1.3$) compared to that of as-prepared sample ($I_D/I_G = 1.15$). After extended cycling (165 cycles) and at charged state, the structure became progressively less ordered ($I_D/I_G = 1.2$) compared wtih its initial state, but still more ordered than that of the discharged state. The results indicate that defects in $sp^2$ carbons are altered during Na insertion/extraction. Moreover, a previous study[28] using elemental analysis and energy dispersive spec-

troscopy (EDS) measurements, indicated that the carbon made from $CO_2$ is a structure with defects, arising from heterogeneously distributed oxygen groups, comprising about 3–4% of the material. Amorphous and turbostatic carbons show promising performance as anodes in LIBs.[30–33] This type of carbon is capable of accommodating more Li ions in disordered interlayers as well as micropores. Hence, it is highly possible that the defects in this material promote Na-ion insertion.

To investigate the electrochemical charge storage behavior of the dMLG electrode, we carried out cyclic voltammetry (CV) and galvanostatic charge/discharge cycling (Figure 3). Samples were cycled between 3.0 and 0.01 V versus $Na/Na^+$ in CV and 2.5 and 0.01 V in galvanostatic charge/discharge cycling. In the first negative scan of the CV (Figure 3D), there is a broad irreversible peak with an onset potential near 1.0 V, which is attributed to the decomposition of the electrolyte and formation of solid electrolyte interphase (SEI) on the surface of carbon.[16,24] In the subsequent cycles, the CV curves almost overlap, suggesting that capacity loss occurs at the initial cycle and subsequently the electrode exhibits reversibility and stability in terms of $Na^+$-ion insertion and extraction. There are two distinct pairs of redox peaks in the voltammogram: 1) a pair of

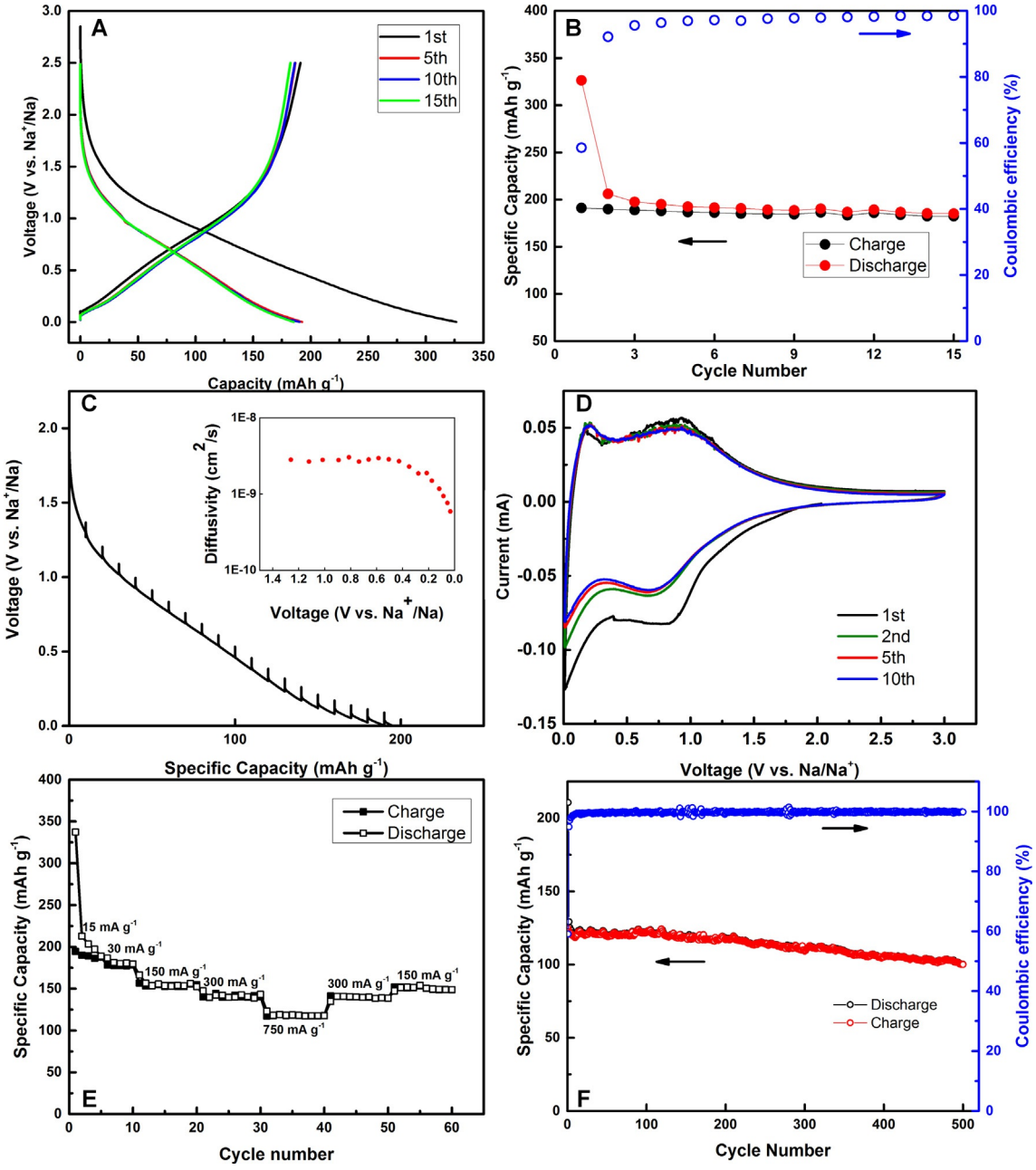


**Figure 3.** Electrochemical characterization and battery performance of the dMLG as anode material for Na-ion batteries. (A) Charge/discharge voltage profiles of the electrode at 2.5–0.001 V and (B) low-rate performance at a current rate of 15 mA $g^{-1}$; (C) GITT profile (inset: diffusivity at different states of charge); (D) CVs of the dMLG electrode in 1 M $NaClO_4$ in ethylene carbonate/propylene carbonate (1:1) at a scan rate of 0.1 mV $s^{-1}$; (E) rate capability and (F) cycling performance of the electrode at a current rate of 750 mA $g^{-1}$.

broad peaks over a region of 0.7–0.9 V and 2) a pair of sharper peaks near 0.1 V. These pairs of broad peaks and sharp peaks correspond to the sloping region and the plateau region of the galvanostatic charge/discharge curves (Figure 3A), respectively. The charge from the broad peak is significant compared to that of the sharp peak, which explains that a significant portion (~77%) of the capacity of the electrode is ascribed to the sloping region.

From the voltage profiles shown in Figure 3A, it can be seen that the electrode delivered a specific capacity of 326 mA h $g^{-1}$ at the first discharge and the specific capacity of first charge is of 191 mA h $g^{-1}$, corresponding to a 41% initial irreversible capacity loss. The large irreversible capacity loss is likely a result of decomposition of the electrolyte and formation of a SEI film on the carbon surface, as discussed above. After 15 cycles, the electrode exhibits a reversible specific capacity of ~190 mA h $g^{-1}$ with a Coulombic efficiency of 98.5%. There are two distinct regions in the charge/discharge curves (i.e., a sloping region in the range of 0.9–0.2 V and a small plateau region near 0.1 V). The mechanism of how $Na^+$ ions are stored in the disordered carbon is currently under debate. It was proposed by Dahn et al.[34] over a decade ago that the $Na^+$ storage in hard carbon follows a "house of cards" mechanism. In this model, it is believed that the high-potential sloping region is attributed to insertion of $Na^+$ ions between parallel or nearly parallel graphene layers in the turbostatic structures, whereas the low-potential plateaus are attributed to insertion of $Na^+$ ions into nanoporosity between randomly stacked layers through an adsorption-like process. On the other hand, recent reports on both experimental and theoretical results[24,35–37] suggested that the plateau region is a result of $Na^+$-ion insertion into the interlayer spacing of graphene layers as opposed to the nanopore filling mechanism suggested by the "house of cards" model. It is also suggested that the sloping region is related to $Na^+$ ions binding to the defect sites (e.g., vacancies) on the graphene layers.

In general, a sloping voltage profile is associated with ion insertion into a host structure where the insertion sites have a distribution of energies. A disordered carbon would possesses a wide site energy distribution, and hence a significant portion of its total capacity would be from the sloping region at higher voltage as was the case of the dMLG electrode. DFT work by Shenoy et al.[37] suggests that Na adsorption is thermodynamically unstable compared with Na plating (at 0 V) in pristine (defect-free) graphene, whereas the presence of defects [e.g., di-vacancy (DV), Stone-Wales] enhances the adsorption. Additionally, when the atoms are on and around the defect sites the potential is larger. As a result, such defects may enhance Na intercalation by strong binding energy to overcome the van der Waals (vdW) force between graphene sheets. A more recent ab initio work by Yamada et al.[36] considered the effect of both a larger interlayer distance and the presence of defects on the mechanism of Na intercalation into disordered carbon. Their work suggests that Na can directly intercalate into disordered carbon without the effect of larger initial interlayer distances, especially with mono-vacancy (MV) and DV defects.[36] Moreover, the DFT analysis employing vdW interactions shows that a strong binding energy that corresponds to the Na adsorption on the defective carbon surface and intercalation into disordered carbon would account for the sloping region, whereas the plateau region would be ascribed to the intercalation into sites around the defects. We conducted TEM elemental mapping (Figure S2) on a sodiated electrode (discharged at 2$^{nd}$ cycle) and it is apparent that Na ions had incorporated into the disordered graphene electrode. The ex situ high-resolution TEM of the sodiated sample shown in Figure 2E suggests that the electrode remains disordered and there is no significant change of the interlayer distance. The interlayer spacing of the dMLG is ~3.51 Å as compared with 3.7–3.8 Å of other reported disordered carbons.[16,20,24,35] Therefore, one would expect less $Na^+$-ion intercalation between graphene sheets in this sample, which corroborates well with the very short plateau region with smaller capacity in the discharge curve. To investigate "pore filling" mechanism,[34] we carried out ex situ small-angle X-ray scattering (SAXS) experiments on charged (de-sodiated) and discharged (sodiated) samples. SAXS has been widely used to investigate the nanoporous structure.[38] The intensity of the small angle scattering signal varies with the difference between the scattering power of the carbon matrix and scattering power of the nanopore. As shown in Figure S3, there is no apparent difference in terms of the log intensity in the charged and discharged samples, which suggests that it is less likely that $Na^+$ ions intercalate into the nanopores of the dMLG.

To elucidate the Na-intercalation mechanism, we further investigated the kinetics by galvanostatic intermittent titration (GITT) measurement. The sodium diffusivity in the dMLG electrode is shown as a function of potential (Figure 3C, inset). It shows that the diffusion associated with the sloping region is quite stable and is much faster than that of the plateau region, indicating that Na intercalation occurs on easily accessible sites, such as defects in the disordered carbon structure. Our result is consistent with what was reported on other carbon structures.[35] It is postulated that the defect sites on the surface of graphene are more accessible compared to the interlayer space as $Na^+$ ions would need to overcome the repulsion from Na ions already adsorbed on previous defect sites, as well as the vdW force between graphene sheets, to diffuse further into the interlayer space. As the interlayer space of the dMLG structure is not as large compared with that of desired spacing of larger than 3.7 Å, we observed a steep decrease in diffusivity in the plateau region. Study of the interlayer distance effect on the charge storage property of the 3D graphene is currently underway and will be reported elsewhere.

We also evaluated the rate capability of the dMLG electrode and the rate performance is shown in Figure 3E. The electrode was cycled at a wide range of current rates. This electrode delivered reversible capacities of 190, 181, 153, 140, and 118 mA h $g^{-1}$ at current rates of 15, 30, 150, 300, and 750 mA $g^{-1}$, respectively. The electrode maintained its previous value when it was cycled back from high rate to low rate, indicating stability of the electrode under a wide current range. This result demonstrates that the dMLG electrode exhibits good rate capability even at high current rate.

Figure 3F displays the cyclability of the dMLG electrode at a current rate of 750 mA $g^{-1}$. The electrode maintains a reversible capacity of 122 mA h $g^{-1}$ after 100 cycles, corresponding to a capacity retention of 97.6% and a capacity retention of 80.3% at 500 cycles with a 99.8% Coulombic efficiency. The cycling performance is comparable with that of hollow carbon nanowires.[16] The good cycling performance is possibly a result of the 3D nanostructure to accommodate for the mechanical stress caused by repeated Na-ion insertion/extraction.

In summary, a dMLG electrode was synthesized through direct reaction of $CO_2$. The as-prepared carbon is a disordered structure with defects and is consists of domains of 4–5 stacked graphene layers with an average layer spacing of ~3.51 Å. The dMLG electrode exhibited a low rate capacity of approximately 190 mA h $g^{-1}$ at 15 mA $g^{-1}$ with a sloping region and a short plateau region in the discharge curves. At a high current rate of 750 mA $g^{-1}$, the electrode delivered a reversible capacity of 125 mA h $g^{-1}$ and demonstrated good rate capability and cyclability. Moreover, structural and electrochemical characterizations suggest two types of Na-ion insertion/extraction mechanisms: 1) at a higher voltage range of 0.9–0.2 V, it is suggested that the Na ions are inserted/extracted at the defective carbon surface in the dMLG, whereas 2) at lower voltage range of 0.2–0.001 V, the charge transfer occurs in between graphene layers near the defects. This novel approach to synthesize dMLG from $CO_2$ make it attractive not only as an anode material for SIBs, but also to control $CO_2$ emission. Further improvement in this anode material could be geared toward tailoring the interlayer spacing between graphene sheets.

## Experimental Section

**Synthesis of dMLG**. Synthesis of a novel cauliflower-fungus-like dMLG structure was reported previously.[27] Briefly, Li particles (Aldrich) were loaded into a ceramic tube batch reactor and $CO_2$ was introduced into the reactor with initial pressure of 50 psi (1 psi ≈0.007 MPa) at room temperature, followed by heating the reactor to 550 °C at a rate of 10 °C $min^{-1}$. The target temperature was held for 48 h. The obtained graphene was separated from other solid products by the treatment of 36.5 wt% HCl, de-ionized water washing (more than 10 times), and centrifugation separation. The obtained graphene was dried overnight at 80 °C.

**Materials characterization**. The dMLG samples were subjected XRD measurements using a Scintag XDS-2000 powder diffract meter with CuK$\alpha$ ($\lambda = 1.5406$ Å) radiation. Surface area and pore size distribution were measured with a Micromeritics ASAP 2000 surface area measurement analyzer using nitrogen adsorption at liquid-nitrogen temperature (77 K). Before the nitrogen adsorption measurement, the sample was degassed at 100 °C. The morphology of samples were investigated by SEM with a JEOL JSM-7500F Field Emission SEM operating at 10 kV. High-resolution TEM images and elemental mapping of energy-filtered TEM were obtained using a JEOL JEM2100F equipped with a field emission gun operated at 300 kV. Raman analysis was conducted with a Renishaw inVia confocal Raman microscope using an Yg-Nd laser (514 nm) with 10% laser power.

**Electrochemical testing**. Electrodes were prepared with carboxymethyl cellulose (CMC, Walocel CRT 20000 PA, Dow Chemical Company) binder. A slurry of 90 wt% active material and 10 wt% CMC binder was screen printed on a 100 μm-thick Al current collector using a film coater (MTI Corp.) and then vacuum dried overnight at 110 °C. Na half-cells were assembled in coin-type cells (Hohsen 2032) with a Na-metal foil as the negative electrode, glass fiber separator (Whatman GF/F), and 1 M $NaClO_4$ (Aldrich) in a 1:1 mixture of ethylene carbonate/propylene carbonate electrolyte (BASF). Half-cells were cycled galvanostatically at varying currents between 2.5 and 0.01 V versus $Na/Na^+$, respectively, using an automated Maccor battery tester at ambient temperature. The galvanostatic intermittent titration technique (GITT) measurement was consisted of a series of current pulse of 20 mA $g^{-1}$ for 30 min and a 2 h rest period until the voltage reached a cut-off value of 0.001 V. CVs of a three-electrode cell using flag-type electrodes with Na as both counter and reference electrode was recorded in a CHI660D Potentiostat/Galvanostat between 3.0 and 0.01 V versus $Na/Na^+$ with a scan rate of 0.1 mV $s^{-1}$. Electrodes removed from cells for analysis were thoroughly washed with dry dimethyl carbonate (BASF) and allowed to dry under inert atmosphere. All cell assembly and disassembly operations were performed in an Ar-filled dry glove box ($O_2$ level < 0.5 ppm).

## Acknowledgements

*H. X. acknowledges the support from the Center for Advanced Energy Studies. This work and use of the Center for Nanoscale Materials were supported by the U.S. Department of Energy, USDOE-BES, under Contract DE-AC02-06CH11357. The work at the APS was supported by the US Department of Energy Scientific User Facilities under Contract DEAC02-06CH11357 with U Chicago Argonne, LLC, and operator of Argonne National Laboratory.*

**Keywords:** carbon dioxide mitigation · carbon material · defect · energy storage · sodium-ion battery

[1] C. Wadia, P. Albertus, V. Srinivasan, *J. Power Sources* **2011**, *196*, 1593–1598.
[2] M. D. Slater, D. Kim, E. Lee, C. S. Johnson, *Adv. Funct. Mater.* **2013**, *23*, 947–958.
[3] M. Dahbi, N. Yabuuchi, K. Kubota, K. Tokiwa, S. Komaba, *Phys. Chem. Chem. Phys.* **2014**, *16*, 15007–15028.
[4] S.-W. Kim, D.-H. Seo, X. Ma, G. Ceder, K. Kang, *Adv. Energy Mater.* **2012**, *2*, 710–721.
[5] S. P. Ong, V. L. Chevrier, G. Hautier, A. Jain, C. Moore, S. Kim, X. Ma, G. Ceder, *Energy Environ. Sci.* **2011**, *4*, 3680–3688.
[6] B. L. Ellis, L. F. Nazar, *Curr. Opin. Solid State Mater. Sci.* **2012**, *16*, 168–177.
[7] V. Palomares, P. Serras, I. Villaluenga, K. B. Hueso, J. Carretero-Gonzalez, T. Rojo, *Energy Environ. Sci.* **2012**, *5*, 5884–5901.
[8] X. Xiang, K. Zhang, J. Chen, *Adv. Mater.* **2015**, *27*, 5343–5364.
[9] J. Liu, J. G. Zhang, Z. G. Yang, J. P. Lemmon, C. Imhoff, G. L. Graff, L. Y. Li, J. Z. Hu, C. M. Wang, J. Xiao, G. Xia, V. V. Viswanathan, S. Baskaran, V. Sprenkle, X. L. Li, Y. Y. Shao, B. Schwenzer, *Adv. Funct. Mater.* **2013**, *23*, 929–946.
[10] S. Tepavcevic, H. Xiong, V. R. Stamenkovic, X. B. Zuo, M. Balasubramanian, V. B. Prakapenka, C. S. Johnson, T. Rajh, *ACS Nano* **2012**, *6*, 530–538.
[11] H. Xiong, M. D. Slater, M. Balasubramanian, C. S. Johnson, T. Rajh, *J. Phys. Chem. Lett.* **2011**, DOI: 10.1021/jz2012066.
[12] V. Palomares, M. Casas-Cabanas, E. Castillo-Martinez, M. H. Han, T. Rojo, *Energy Environ. Sci.* **2013**, *6*, 2312–2337.
[13] D. Kim, S. H. Kang, M. Slater, S. Rood, J. T. Vaughey, N. Karan, M. Balasubramanian, C. S. Johnson, *Adv. Energy Mater.* **2011**, *1*, 333–336.
[14] J. Xu, D. H. Lee, R. J. Clement, X. Q. Yu, M. Leskes, A. J. Pell, G. Pintacuda, X. Q. Yang, C. P. Grey, Y. S. Meng, *Chem. Mater.* **2014**, *26*, 1260–1269.

[15] M. M. Doeff, Y. P. Ma, S. J. Visco, L. C. Dejonghe, *J. Electrochem. Soc.* **1993**, *140*, L169 – L170.
[16] Y. L. Cao, L. F. Xiao, M. L. Sushko, W. Wang, B. Schwenzer, J. Xiao, Z. M. Nie, L. V. Saraf, Z. G. Yang, J. Liu, *Nano Lett.* **2012**, *12*, 3783 – 3787.
[17] C. Bommier, X. L. Ji, *Isr. J. Chem.* **2015**, *55*, 486 – 507.
[18] Y. Okamoto, *J. Phys. Chem. C* **2014**, *118*, 16 – 19.
[19] H. Kim, J. Hong, G. Yoon, H. Kim, K. Y. Park, M. S. Park, W. S. Yoon, K. Kang, *Energy Environ. Sci.* **2015**, *8*, 2963 – 2969.
[20] Y. Wen, K. He, Y. J. Zhu, F. D. Han, Y. H. Xu, I. Matsuda, Y. Ishii, J. Cumings, C. S. Wang, *Nat. Commun.* **2014**, *5*, 4033.
[21] D. A. Stevens, J. R. Dahn, *J. Electrochem. Soc.* **2000**, *147*, 1271 – 1273.
[22] R. Alcántara, J. M. Jimenez-Mateos, P. Lavela, J. L. Tirado, *Electrochem. Commun.* **2001**, *3*, 639 – 642.
[23] S. Komaba, W. Murata, T. Ishikawa, N. Yabuuchi, T. Ozeki, T. Nakayama, A. Ogata, K. Gotoh, K. Fujiwara, *Adv. Funct. Mater.* **2011**, *21*, 3859 – 3867.
[24] J. Ding, H. L. Wang, Z. Li, A. Kohandehghan, K. Cui, Z. W. Xu, B. Zahiri, X. H. Tan, E. M. Lotfabad, B. C. Olsen, D. Mitlin, *ACS Nano* **2013**, *7*, 11004 – 11015.
[25] Z. H. Wang, L. Qie, L. X. Yuan, W. X. Zhang, X. L. Hu, Y. H. Huang, *Carbon* **2013**, *55*, 328 – 334.
[26] J. T. Xu, M. Wang, N. P. Wickramaratne, M. Jaroniec, S. X. Dou, L. M. Dai, *Adv. Mater.* **2015**, *27*, 2042 – 2048.
[27] W. Wei, K. Sun, Y. H. Hu, *J. Mater. Chem. A* **2014**, *2*, 16842 – 16846.
[28] L. Chang, W. Wei, K. Sun, Y. H. Hu, *J. Mater. Chem. A* **2015**, *3*, 10183 – 10187.
[29] C. Portet, G. Yushin, Y. Gogotsi, *Carbon* **2007**, *45*, 2511 – 2518.
[30] J. R. Dahn, T. Zheng, Y. H. Liu, J. S. Xue, *Science* **1995**, *270*, 590 – 593.
[31] T. Zheng, Y. H. Liu, E. W. Fuller, S. Tseng, U. Vonsacken, J. R. Dahn, *J. Electrochem. Soc.* **1995**, *142*, 2581 – 2590.
[32] T. Zheng, J. N. Reimers, J. R. Dahn, *Phys. Rev. B* **1995**, *51*, 734 – 741.
[33] V. Etacheri, C. W. Wang, M. J. O'Connell, C. K. Chan, V. G. Pol, *J. Mater. Chem. A* **2015**, *3*, 9861 – 9868.
[34] D. A. Stevens, J. R. Dahn, *J. Electrochem. Soc.* **2001**, *148*, A803 – A811.
[35] C. Bommier, T. W. Surta, M. Dolgos, X. Ji, *Nano Lett.* **2015**, *15*, 5888 – 5892.
[36] P. C. Tsai, S. C. Chung, S. K. Lin, A. Yamada, *J. Mater. Chem. A* **2015**, *3*, 9763 – 9768.
[37] D. Datta, J. W. Li, V. B. Shenoy, *ACS Appl. Mater. Interfaces* **2014**, *6*, 1788 – 1795.
[38] G. O. Park, J. Yoon, E. Park, S. B. Park, H. Kim, K. H. Kim, X. Jin, T. J. Shin, H. Kim, W. S. Thon, J. M. Kim, *ACS Nano* **2015**, *9*, 5470 – 5477.

Received: January 27, 2016
Revised: March 3, 2016
Published online on April 28, 2016